NASA TN D-1217

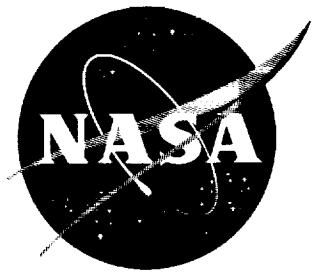

TECHNICAL NOTE

D-1217

HIGH-VACUUM CONDENSER DESIGN: EXPERIMENTAL EFFECTS FROM CESIUM AND MERCURY ION BEAMS

By Edward A. Richley and Ronald J. Cybulski

Lewis Research Center
Cleveland, Ohio

NATIONAL AERONAUTICS AND SPACE ADMINISTRATION
WASHINGTON

August 1962

NATIONAL AERONAUTICS AND SPACE ADMINISTRATION

TECHNICAL NOTE D-1217

HIGH-VACUUM CONDENSER DESIGN: EXPERIMENTAL EFFECTS FROM CESIUM AND MERCURY ION BEAMS

By Edward A. Richley and Ronald J. Cybulski

SUMMARY

Effects of variable-energy electrostatic rocket-engine ion exhaust beams that pertain to the design of high-vacuum condensers are discussed. Three ion-engine beam sources, using cesium and mercury as propellants, were operated at energy levels of 200 to 9000 electron volts and currents of 0.002 to 0.200 ampere. Five condenser geometries, having surface areas from 0.267 to 5.76 square meters, were tested. Values for a function of the accommodation and condensation coefficients, which appears in an existing theoretical analysis, were determined. Although exhibiting rather wide variations in some tests, the values were estimated at approximately 0.15 for cesium and 0.015 for mercury. A method of estimating condenser surface area requirements is given.

INTRODUCTION

Recent advances in the field of electric propulsion have led investigators to consider larger and larger vacuum facilities for the testing of electric rocket engines. Two such facilities, for example, are presently under construction at the NASA Lewis Research Center. One is a 25-foot-diameter by 80-foot-long tank, and the other is a 15-foot-diameter by 60-foot-long tank (see ref. 1).

To maintain the pressure levels desired for adequate testing of electric rocket engines, the high-vacuum facility must provide a means of handling the rocket exhaust products. Space environmental simulation in which collision processes between the ion rocket beam and the ambient chamber molecules are negligible makes facility pressures of the order of 1×10^{-6} millimeter of mercury or lower desirable (see ref. 2). Facility geometry and economic considerations make a combination of oil diffusion pumps and refrigerated condensing surfaces appear attractive (ref. 3).

With this scheme, the refrigerated condensing surfaces or condensers would be used to remove the condensable rocket exhaust products, and the diffusion pumps would be used to evacuate and remove the noncondensables in the test system.

The facility in operation is shown typically in the following sketch:

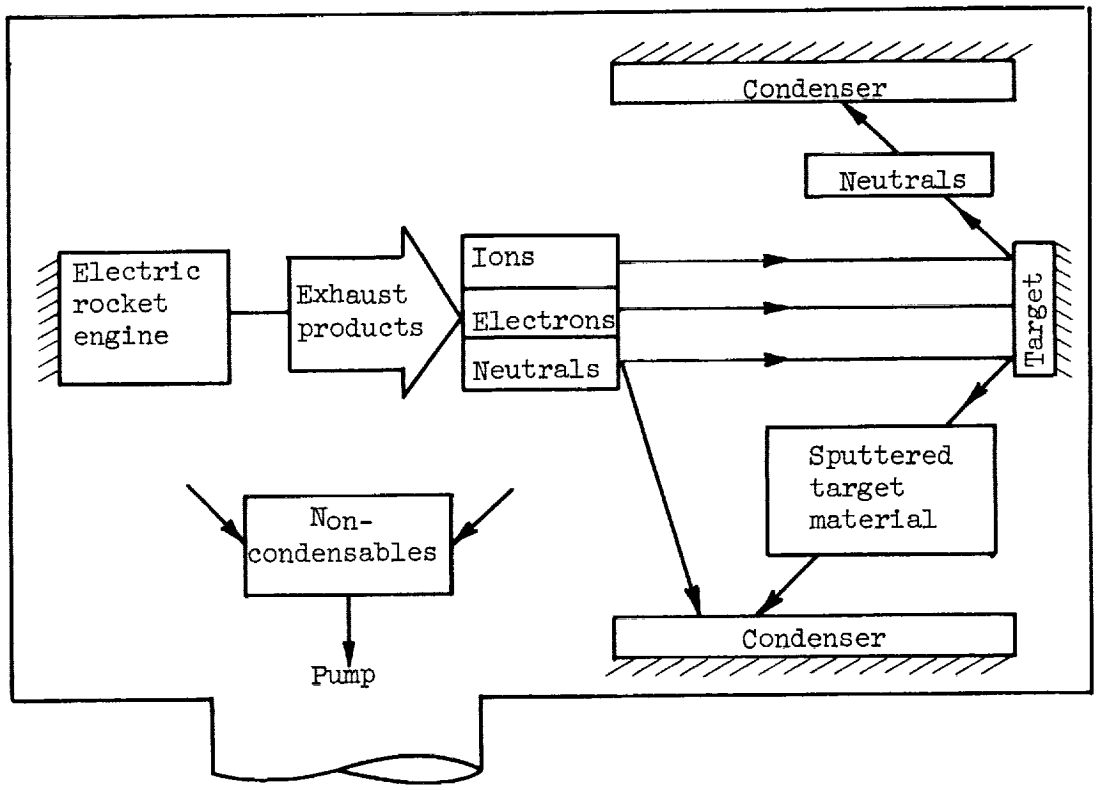

Noncondensables are present from the ambient atmosphere in the facility, from outgassing of heated components of the engine, and from removal of surface films by the engine exhaust. They are removed or maintained at a low density by the pump. The engine exhaust products may consist of ions, electrons, and neutral particles. The percentage of neutral particles is usually low, as is their energy level, and their presence poses no serious condensation problem. Electron and ion impingement on the target may give rise to low-energy sputtered material which must be condensed. In addition, the rebounding "neutralized" particles that result from ion collisions with the target and which may have a high energy content must be condensed. The condensation of these neutralized particles is the basic problem of condenser design.

The mechanism of condensation is complex. Although it has been studied in some detail by investigators working with small-scale laboratory experiments, very little information has been compiled, theoretical or experimental, describing the process in terms adequate for application to the design of condensers for large-scale facilities.

This report presents the results from condenser tests which utilized the ion exhaust beams from prototype electrostatic ion rocket engines. The engines used cesium or mercury vapor for the propellant. The work was conducted as part of a program to obtain condenser design information for the two facilities mentioned previously, and results are presented in a form that may be useful to other investigators working in the field of condenser design. In the tests, cesium ion beam currents of from 0.002 to 0.012 ampere at energy levels of from 200 to 9000 electron volts, and mercury ion beam currents of from 0.025 to 0.200 ampere at 2500 to 6000 electron volts were used. Five condenser geometries having surface areas of from 0.267 to 5.76 square meters were tested. Parameters monitored included beam current and potential, condenser temperature, and the variation of pressure with time. Potentials are referenced to facility ground.

Results are presented in terms of the theoretical development of reference 4. Although presented primarily for its heuristic value, reference 4 does describe the condenser design problem in terms of parameters of interest, namely, beam velocity, propellant mass-flow rate, pressure, condenser surface area, and a function of the propellant accommodation and condensation (or sticking) coefficients. The relation among these parameters along with a summary of the process as described in reference 4 is given in the section entitled THEORY. The difficulty in using the equations of reference 4 for condenser design stems from the unavailability of reliable values of accommodation and/or condensation coefficients for the various elements.

The low-energy sodium molecular beam tests of reference 5 were similar to the work reported herein in that an attempt was made to evaluate the empirical function of reference 4 for sodium. Several comparisons will be made between the results of reference 5 and those now being reported for cesium and mercury.

SYMBOLS

a	accommodation coefficient, dimensionless
e	particle charge, 1.6019×10^{-19} coulomb
$F(a,f)$	function of a and f, dimensionless
F^*	function of a, f, and G, dimensionless

f	condensation coefficient, dimensionless
G	ionization gage correction factor, dimensionless
J	current, amp
m	molecular mass, kg
N	particle flow rate, particles/sec
n	number of rebounds, dimensionless
p	pressure, mm Hg
Δp	true pressure difference, mm Hg
Δp^*	indicated pressure difference, mm Hg
S	surface area, sq m
V	potential difference, volts
v_j	initial velocity, m/sec
$v_{0,\ldots,n}$	rebound velocity, m/sec

Subscript:

i	1, 2, . . ., 5

THEORY

The theoretical analysis of reference 4 forms a basis for the calculation of the surface area required for condensation of high-velocity vapor beams in free molecule flow, provided values of the accommodation and condensation coefficients of the propellant are known. Several conditions and assumptions are required to establish the highly idealized model used for the analysis. One significant assumption, for example, is that the condenser geometry is such that shadowing effects are negligible. For the convenience of the reader, a brief summary of the process described in reference 4 follows.

The incoming beam is assumed to hit a target with an initial velocity v_j. Some of the molecules (or ions) may stick as expressed by a condensation coefficient f. The remainder of the molecules rebound with a velocity v_0, having lost some kinetic energy as expressed by a kinetic energy

accommodation coefficient a. These molecules then hit other surfaces, rebounding with a velocity v_1, and so on to v_n, the molecular velocity corresponding to the condensation temperature. Surface area must be provided to the extent that during the n rebounds required to reach condensation conditions, the pressure in the test facility will be maintained at a tolerable level. The analysis considers the total pressure force exerted on the condenser surface as the summation of all momentum changes except that at the target area, which is regarded as a small portion of the total condenser surface area. From momentum considerations then, and where the condenser surface temperature is much less than the propellant condensation temperature, an expression for the force per unit area, the pressure, is developed:

$$133.3\ \Delta p = \frac{2Nmv_j}{3S} F(a,f) \tag{1}$$

where $F(a,f)$, a function of the accommodation and condensation coefficients, is given as

$$F(a,f) = \left[1 + (1 - f)(1 - a)^{1/2}\right]\left\{\frac{(1 - f)(1 - a)^{1/2} - \left[(1 - f)(1 - a)^{1/2}\right]^n}{1 - (1 - f)(1 - a)^{1/2}}\right\} \tag{2}$$

The value 133.3 is a conversion constant for pressure from meter-kilogram-second units (newtons/sq m) to millimeters of mercury.

Further, the analysis notes that for values of $(1 - f)(1 - a)^{1/2} \ll 1$ equation (2) simplifies to

$$F(a,f) = \left[1 + (1 - f)(1 - a)^{1/2}\right](1 - f)(1 - a)^{1/2} \tag{3}$$

This assumption would hold, for example, were $a > 0.9$ and at the same time $f > 0.7$. Values of a and f are anticipated to be in this range in many instances and would seem to justify the simplifying assumption. In this form it is possible, from experimental values of $F(a,f)$, to estimate values of a or f if one or the other is known.

It should be reemphasized that the analysis is based upon a highly idealized model. Additional items that are neglected include condenser sputtering effects, condenser material, and condenser surface condition.

For purposes of experimental data presentation it is to be noted that since

$$N = \frac{J}{e} \tag{4}$$

$$v = \sqrt{\frac{2e}{m} V} \tag{5}$$

equation (1) may be written

$$F(a,f) = 141.3 \sqrt{\frac{e}{m}} \frac{S \Delta p}{J\sqrt{V}} \tag{6}$$

In recognition of a possible pressure-gage correction factor G due to the presence of metal vapors, equation (6) may be written

$$F^* = 141.3 \sqrt{\frac{e}{m}} \frac{S \Delta pG}{J\sqrt{V}} = 141.3 \sqrt{\frac{e}{m}} \frac{S \Delta p^*}{J\sqrt{V}} \tag{7}$$

where Δp^* is the "indicated" gage pressure difference.

APPARATUS

Vacuum Facilities

Three vacuum test chambers were used in the program. Two of the chambers were 16 feet long and 5 feet in diameter, the third was 7 feet long and 3.5 feet in diameter. They were all of stainless steel construction with a hinged door at one end which supported a smaller diameter engine mounting chamber. A view of one of the facilities is shown in figure 1. Oil diffusion pumps with appropriate backup pumps evacuated the chambers to desired background pressure levels. The facilities are described in detail in reference 1.

Ion Beam Sources

Three electrostatic rocket engines were used to supply the ion exhaust beams for the tests. The engines have all been discussed in the literature. Two of the engines, denoted herein as engines A and B, use cesium vapor as a propellant and are known as contact-ionization electrostatic rocket engines. Both are subclassified as the reverse-feed type. Engine A, discussed in reference 6, delivered beam currents up to 0.012 ampere at energy levels up to 1000 electron volts. Engine B is similar

to the engine discussed in reference 7 and supplied beam currents up to 0.007 ampere at up to 9000 electron volts. Engine C, which used mercury vapor as a propellant, is known as an electron-bombardment electrostatic rocket engine. The principle of operation is discussed in reference 8. This engine delivered up to 0.200 ampere of beam current at a 6000-electron-volt energy level.

Engines A and B were mounted in the engine chamber shown in figure 1; while engine C, a somewhat larger engine, was mounted on the facility door. The arrangement of the engines with respect to the test condensers into which the beams were exhausted is shown schematically in figure 2.

Condensers

Two basic condenser configurations, differing primarily in overall size, were utilized with the various engines. One measured 12 by 12 by 18 inches deep with a 45° wedge-shaped target area at the rear. The other was similar in shape and measured 6 by 6 by 18 inches deep. The purpose of the wedge-shaped target area was to deflect the incoming beam to the side walls. The condenser coolant, liquid nitrogen or water, was passed through copper tubing that was brazed to the outer walls. The condensers were made of copper. Inner-wall configurations could be altered, and those geometries tested included: plain wall, full honeycomb, partial honeycomb, and finned. The honeycomb was copper and measured 0.375 inch across the flats by 0.75 inch in height; fins were 1.625 inches high. Figure 3 shows the various configurations and notes the inner-wall surface areas. For convenience, this information, along with the engine used with each condenser, is tabulated as follows:

Condenser				Engine tested
Figure	Symbol	Area, sq m	Description	
3(a)	S_1	0.64	Plain wall (large)	A,B,C
3(b)	S_2	2.86	Partial honeycomb	A,B,C
3(c)	S_3	5.76	Full honeycomb	A,C
3(d)	S_4	1.57	Finned	B
	S_5	.27	Plain wall (small)	B

A collector ring, electrically isolated from the condenser, was used to estimate the stray beam current that may not have entered the condenser because of beam spreading. The location of the collector ring is shown in figure 2.

Instrumentation

Ion beam currents and accelerating potentials were read from meters having 3 percent of full-scale accuracy. Multiple shunt circuits were used in conjunction with the meters to assure readability over a wide range of engine operating conditions. Current to the collector ring was metered in a similar manner.

Condenser temperature was monitored at three different points: the center of the wedge and at the midpoint of the two sides. Copper-constantan thermocouples were used, and the temperatures were read from a self-balancing potentiometer.

Two pressure gages (Bayard-Alpert type ionization gages) were located similarly in each condenser (see fig. 3(a)). The orientation of the gages, transverse to the entering beam axis, prevented direct entry of the beam into the gages. Indicated pressures were read on standard sensing units.

PROCEDURE

The stepwise procedure of a typical test with any of the three ion engines was as follows:

(1) With the engine in place, the facility was evacuated by means of the pumping system. The condenser was then cooled to operating temperature with either liquid nitrogen or water. Ionization gages were degassed, and pressures were recorded until equilibrium was established.

(2) Preliminary heating of engine components was accomplished. The procedure varied slightly among the three engines. For engines A and B this step consisted of heating the propellant vaporizer and ionizer to operating temperature. For engine C, the electron-emitting filament and vaporizer were heated. A time-dependent pressure change, which was recorded until the dependency was clearly established, occurred in the condenser in each case.

(3) The ion beam was started. The engine parameters of potential and current were varied. Condenser temperature and pressure-time dependency were noted for the period of the test.

(4) Propellant flow was stopped. The flow of ions ceased, and the pressure-time dependency was recorded until the curve of step (2) was reestablished.

Upon completion of each test the condenser was removed, cleaned (or the geometry was changed), and prepared for the next test.

RESULTS AND DISCUSSION

A total of 10 tests, using liquid nitrogen as the condenser coolant, were conducted with the three ion beam sources and the various condenser geometries. Some of the tests were repeated using water as the coolant. Running time was varied from 1 to 5 hours.

Figure 4 shows the variation of pressure with time for two typical tests. Figure 4(a) shows the variation of pressure with time for a plain-wall condenser test with engine A. Pressure-time curves for engine B were similar except for a period in two tests during which difficulty in establishing stable operation of the engine occurred. Numbers (1) to (4) on the figure are associated with the stepwise procedure previously outlined. A typical pressure-time curve for engine C is shown in figure 4(b).

Extending the pressure-time curve of step (2) to that of step (4) forms a base line for step (3). The pressure contribution Δp^* of the cesium or mercury vapor was taken as the difference between this base curve and the upper curve of step (3). The two ionization gage readings were averaged for this calculation. Calculated values of F^* were then obtained from these data by use of equation (7).

The sharp rise and relatively rapid decay of pressure with time in the initial period of step (3) were peculiar to practically all the tests and were similar to those observed with the sodium vapor tests reported in reference 5. The subsequent asymptotic leveling out of pressure when ion beam current and energy level were constant was also characteristic of all tests. This portion of the curve is actually quite similar in appearance to the outgassing-type curves commonly observed in connection with conventional vacuum work. The mechanisms involved in these tests, however, were somewhat more complicated, and it is of interest to comment on their possible relative magnitudes.

It is well known that the condensation of metal vapors is a complex process involving adsorption, nucleation, and surface duffusion (see ref. 10). High incident energy levels of the ion exhaust beams suggest additional complications. Any adsorbed gas film on the condenser surfaces, for example, may be removed by the incident ion beam. The pressure contribution, if any, from these gases would add to the initial

pressure rise. The gases could either flow out of the condenser or readsorb on some other portions of the condenser. An exact determination of the extent of this effect requires a knowledge of the gas film thickness and composition, the film-atom per beam-ion removal rate, the gas flow rate, if any, out of the condenser, and the fraction of the condenser surface upon which the ion beam is incident. Since the gas film removal would only occur in the vicinity of the condenser upon which the ion beam impinged, it is likely that many particles would readsorb on other portions of the condenser.

If it could be assumed that the ion beam would remove a certain number of particles of adsorbed gas, say x_0, giving rise to a pressure p_0 in the condenser at time zero, and further that these particles then flow out of the condenser under conditions of free molecule flow, it is possible from basic kinetic theory relations to make a rough estimate of the pressure contribution p in the condenser at time t. The calculation is as follows:

The particle flow rate out of the condenser is

$$-\frac{dx}{dt} = \frac{1}{4} n\bar{v}KA$$

where

n particle number density

$\bar{v}$ average particle velocity

K Clausing factor

A cross-sectional area of condenser

Let $n = x/V$, where V is the condenser volume, and integrate to obtain

$$\frac{x}{x_0} = \exp\left(-\frac{\bar{v}}{4V} KAt\right)$$

or, in terms of pressure,

$$\frac{p}{p_0} = \exp\left(-\frac{\bar{v}}{4V} KAt\right)$$

Now, A = 0.09 square meter, V = 0.03375 cubic meter, and K ≈ 1. Assuming $\bar{v}$ = 100 meters per second and substituting yield

$$\frac{p}{p_0} = \exp(-66.7\ t)$$

From this rough calculation it can be seen that after only 1 second $p \ll p_0$, and it seems unlikely that the removal of any adsorbed gas film would be a contributing factor to the observed pressure-time characteristics of the tests.

Another factor is the possible outflow of propellant from the condenser. Very rough calculations were made for the liquid-nitrogen-cooled tests, which showed the ratio of the outflow to inflow could be as high as 30 percent for the cesium tests and 9 percent for the mercury tests. In making the outflow calculation, which was based on the free molecular flow relation, the flow area was assumed to be the cross-sectional area of the condenser; the Clausing factor was assumed to be unity; no directional pressure effects were considered; and the average particle temperature was estimated at 400° K. It is likely that the actual outflow-to-inflow ratio would be considerably less than the values estimated and would at least be well within the accuracy of the overall test data.

While physical sputtering of the condenser material, as well as the selection of the condenser material itself, may be important, no attempt was made to evaluate these effects.

The ionization gage readings during step (3) could be questioned since the ambient atmosphere now consisted of partial pressure contributions by metal vapors. The ordinary problems of interpretation of ion gage pressure readings are further complicated by the presence of these metal vapors. The deposition of metal atoms on the ion collector could result in a lowering of the work function of the collector. This in turn could result in an increase in photo emission of electrons from the collector because of impingement of light originating from the hot filament and because of soft rays produced by ionizing electrons falling into the helical grid. No attempt was made to determine the extent of this effect in the tests with cesium and mercury; however, in reference 5, tests conducted with partial sodium vapor atmospheres indicated these effects to be negligible at the pressure levels of the tests. The work of reference 9 seems to concur with this view. Gage sensitivity in various atmospheres is also a possible source of error. However, no data on the magnitude of this effect in mixtures of gases are known to the authors, and consequently no correction for sensitivity has been made.

Finally, the initial condenser surface condition - difficult to control in large-scale tests - could be an important factor. Surface contamination, by diffusion pump oil, for example, could appreciably retard

the condensation process. The degree of retardation would tend to diminish with time as more and more propellant came into contact with the condenser surface. This phenomenon of a conditioning of the condenser surface would be directly reflected in the behavior of the pressure-time curves. From the data it might be reasonably concluded that, after the initial sharp pressure rise in step (3), the trend toward a leveling out of pressure, at constant ion beam current and potential, was primarily the result of this conditioning of the condenser surface. The effect can be seen in figure 4. See, for example, the first and last portions of step (3) in figure 4(a). This conclusion, expressed in terms of the condensation coefficient, would be that the value of f increases with time until such time that it attains some equilibrium value. The equilibrium value of f would probably be near unity since it is well documented that condensation coefficients for vapor condensing on a surface composed of the same material have values near unity. The conclusion is also consistent with the findings of reference 5.

Although the theoretical development of reference 4 is highly idealized, equation (7) could be useful for approximating condenser surface area requirements for given values of J, V, and Δp, provided steady-state values of F^* were known. Experimental attempts to determine F^*, however, require the arbitrary selection of an area S. In addition, the area selected must be distributed so as to be fully effective during the test. In connection with this, reference 11 contains an interesting discussion on condenser geometry design using computer techniques. Variations in F^* would be expected if the geometry specified resulted in portions of the condenser being ineffective, that is, shadowing effects.

Figure 5 shows the variation of F^* with time for the three ion beam sources when liquid nitrogen was used as the coolant. Each figure includes data from at least three different condenser geometries and various energy levels as noted. Calculations were based upon actual condenser area. In the tests with engines A and B, wide variations in F^* are exhibited for different condenser areas (figs. 5(a) and (b)). The S_2 and S_4 curves of figure 5(b) are displaced to the right because of the difficulty encountered in these two tests in establishing stable operation of the engine. The problem was internal to the engine. The beam current from engine A was limited by the temperature of the propellant vaporizer and was independent of the accelerating potential. The beam currents from engines B and C, however, were dependent on the accelerating potential. The upper and lower limits of beam current along with the average value for the indicated accelerating potential are shown on figure 5.

In an attempt to discover the relative effectiveness of the various condensers, from the viewpoint of area considerations alone, values of F_i^* of figure 5 were multiplied by the area ratio S_1/S_i where S_1 is

the area of the plain-wall condenser. These values are shown with respect to time in figure 6. The data for engine A indicate very little spread and would suggest that the additional area of the S_2 and S_3 condensers was highly ineffective. The data for engine B are somewhat more difficult to analyze because of the aforementioned difficulties. However, exclusive of the time displacements of the engine B data, the curves do seem to be approaching a common asymptotic value. The short S_5 curve of figure 5(b) is displaced in figure 6 above the maximum value of the ordinate and is not shown. The curves of figure 6 for engines A and B suggest a possible equilibrium value of F^* for cesium of about 0.15.

The curves of engine C, although appearing asymptotic, do not exhibit quite the same characteristics. Asymptotic values of F^* are small; however, if the end points of each curve are examined and considered to be nearly the equilibrium value, displacements among the three curves can be seen. The S_1/S_3 curve is about one-third that of the S_1/S_1 curve, and the S_1/S_2 curve is about one-half that of the S_1/S_1 curve. These relative ratios are much greater than any observed in the engine A and B tests and tend to indicate that the additional area of the S_2 and S_3 condensers was at least partially effective in the engine C tests. This area effect will be made more evident in the discussion of figure 7 which follows. The engine C tests were conducted at much higher propellant mass-flow rates, and possibly because of this portions of the condensers that were not effective in the engine A and B tests were being utilized.

Figure 7 shows the variation of pressure differential with time for each test. The steplike changes occurring are a result of changes in ion beam energy and/or beam current (see fig. 5). It is interesting to note that in figures 7(a) and (b) the pressure levels do not appear to be strongly influenced by changes in condenser area. However, in figure 7(c) pressure levels are progressively lowered by the addition of more condenser area. This would again seem to demonstrate that additional surface area was not effective with engines A and B but, to some extent, was effective with engine C. The extent of the effectiveness is difficult to evaluate quantitatively.

Figure 8 is a view of the condenser S_3 after testing with engine C. Visual observation shows the rear portions to appear clean, while the honeycombs toward the front are discolored from mercury. Deep down in all the honeycombs, out of a direct line of sight with the beam, discolorations also indicated some evidence of condensate. This would imply that the cleaned portions were possibly acting as a deflection target, but not doing any condensing. Thus, while it is possible to postulate a very rough value of F^* for mercury from figure 5(c) to be near 0.015, additional work is required to investigate more fully the effects of condenser geometry.

Reference 5 gives a range of values of F^* for sodium of 0.12 to 0.04, with 0.04 as the more likely value. The values suggested from the work herein of 0.15 for cesium and 0.015 for mercury seem to be reasonably within the same range.

In the aforementioned tests, the condenser surface temperature was near that of liquid nitrogen - much lower than the condensation temperature of cesium or mercury. Tests were also conducted using tap water as a condenser coolant. Water temperature varied between 60° and 80° F for the tests.

Comparisons of step (3) of the pressure-time curves with the two coolants are shown in figure 9. The tests with cesium (fig. 9(a)) show little difference between the two, while the tests with mercury (fig. 9(b)) show considerable difference. The results seem consistent with what might be anticipated from examining the equilibrium vapor pressure-temperature curves of cesium and mercury. Reference 12 shows the vapor pressure of mercury over the temperature range indicated previously to be 1.3 to 2×10^{-3} millimeter of mercury and that of cesium to be 6.2×10^{-7} to 1.8×10^{-6} millimeter of mercury. While the cesium data seem to fall within this range, the indicated pressure in the engine C (mercury) tests is lower than the vapor pressure data. The reason for this apparent discrepancy in the mercury tests may, in this case, be due to mercury outflow from the condenser. Clearly though, for the conditions tested, liquid-nitrogen cooling appears much more important with mercury than with the cesium tests.

As indicated in the INTRODUCTION, one primary object of the tests was to obtain condenser design information applicable to the two large facilities currently under construction at the Lewis Research Center. The values found for F^*, when used with equation (7), would appear adequate for a first approximation of surface area requirements. These values are given in a convenient form for estimating surface area requirements in figure 10. Figure 10 shows the variation of $141.3\sqrt{e/m}\,S\,\Delta p^*$ with $JV^{1/2}$. The solid curves shown were calculated from the specific values of F^* of 0.15, 0.04, and 0.015. These are the values of F^* previously found to be representative of the cesium, sodium, and mercury data, respectively. The data points shown on figure 10 are the actual data with no attempt made to assign an effective condenser area. Data from reference 5 for sodium are also shown. The data points are included in figure 10 to demonstrate both the trend of the data and to illustrate the difficulty encountered in interpreting the data.

Figure 10 may be used to estimate condenser surface area requirements as illustrated in the following example. Consider the surface area requirements for an electrostatic ion rocket engine using cesium vapor as a propellant and operating at a thrust level of 1.23 newtons. This

corresponds to a beam power of 30 kilowatts and a specific impulse of 5000 seconds (V of 1650 volts). Let it be further assumed that the facility background pressure is 1×10^{-6} millimeter of mercury and that the maximum pressure rise Δp^* tolerable in the facility is 1×10^{-6} millimeter of mercury. Then, J will be 18.2 amperes and $JV^{1/2}$ will be $740(\text{amperes})(\text{volt})^{1/2}$. Enter figure 10 as shown by the dashed line and obtain the value of the ordinate to be 111, from which the surface area requirement is found to be 383 square meters - an appreciable area - and indicative of the importance of condensers in electric-rocket-engine test facilities.

As a further application, under the assumption that the specified values of F^* may be approximately equal to $F(a,f)$, these values could be used in equation (3) to estimate values of the sticking coefficient f for the various propellants. Of course, a further assumption of the accommodation coefficient is required. In this manner a sticking coefficient of approximately 0.75 was estimated for sodium in reference 5.

It is to be reemphasized that no absolute degree of certainty can be associated with estimates from figure 10. Based on the previous discussion of the data, it is the opinion of the authors that the solid curves shown on figure 10 are possibly closer to the true values.

CONCLUDING REMARKS

To study the effects from cesium and mercury ion beams on condenser design, five condenser geometries were tested. Parameters studied included pressure, condenser surface area, beam potential (velocity), and beam current (mass-flow rate).

In the initial stages of engine operation all tests showed a strong pressure-time dependency, which suggests the occurrence of a condenser surface conditioning effect. The large initial pressure rise may be a severe limitation to the testing of full-scale electric rocket engines.

Specification of the optimum condenser geometry remains as a problem. The tests with cesium beams showed little effect of additional surface area over that of the plain-wall condenser and suggest that the simplest geometry may be the most effective. However, the mercury tests, which were conducted at higher mass-flow rates, indicated the honeycomb geometry to be more effective.

It was found that the required condenser temperature to maintain a tolerable pressure rise can be approximated from the vapor pressure curves for the propellant under consideration and a knowledge of the

facility background pressure. It has been demonstrated that, for metal vapors with vapor pressures at room temperature that are of the order of the facility background pressure, circulating water may be adequate as a condenser coolant.

Although the theoretical analysis of reference 4 is highly idealized, values of F^* for cesium (0.15), mercury (0.015), and sodium (0.04, from ref. 5) vapor have been obtained that should be useful in equation (7) for first-order approximation of surface area requirements for condensers in large vacuum facilities. Using the value obtained for cesium, an ion engine operating at 1.23-newtons thrust was estimated to require on the order of 400 square meters of condensing surface.

Lewis Research Center
National Aeronautics and Space Administration
Cleveland, Ohio, March 12, 1962

REFERENCES

1. Keller, Thomas A.: NASA Electric Rocket Test Facilities. Seventh Nat. Symposium on Vacuum Tech. Trans., Pergamon Press, 1960, pp. 161-167.

2. Kaufman, Harold R.: The Neutralization of Ion-Rocket Beams. NASA TN D-1055, 1961.

3. Childs, J. H.: Design of Ion Rockets and Test Facilities. Paper 59-103, Inst. Aero. Sci., 1959.

4. Mickelsen, W. R., and Childs, J. H.: Theoretical Analysis of Ultra-high Vacuum Condensers. Rev. Sci. Instr., vol. 29, no. 10, Oct. 1958, pp. 871-873.

5. Richley, Edward A., Cybulski, Ronald J., and Keller, Thomas A.: Experimental Evaluation of High-Vacuum Condensers in Large Vacuum Facilities. Paper presented at Int. Organization Vacuum Sci. and Tech., Wash., D.C., Oct. 16-19, 1961.

6. Childs, J. Howard, and Mickelsen, W. R.: Grid Electrode Ion Rockets for Low Specific Impulse Missions. Paper presented at Second AFOSR Symposium on Advanced Prop. Concepts, Boston (Mass.), Oct. 7-9, 1959.

7. Dangle, E. E., and Lockwood, D. L.: NASA Experimental Research with Ion Rockets. Preprint 1126-60, Am. Rocket Soc., Inc., 1960.

8. Kaufman, Harold R.: An Ion Rocket with an Electron-Bombardment Ion Source. NASA TN D-585, 1961.

9. Redhead, P. A.: Errors in the Measurement of Pressure with Ionization Gauges. Seventh Nat. Symposium on Vacuum Tech. Trans., Pergamon Press, 1960, pp. 108-111.

10. Yang, L., Birchenall, C. E., Pound, G. M., and Simnad, M. T.: Some Observations on Heterogeneous Nucleation of Sodium Crystals from Atomic Beams. Acta Metallurgica, vol. 2, 1954, pp. 462-469.

11. Santeler, Donald: Theory and Design of Cryogenic Pumping Systems for Space Environmental Simulators. Second Annual Symposium on Space Vacuum Simulation, Arthur D. Little, Inc., June 16, 1961.

12. Honig, R. E.: Vapor Pressure Data for the More Common Elements. RCA Rev., vol. XVIII, no. 2, June 1957, pp. 195-204.

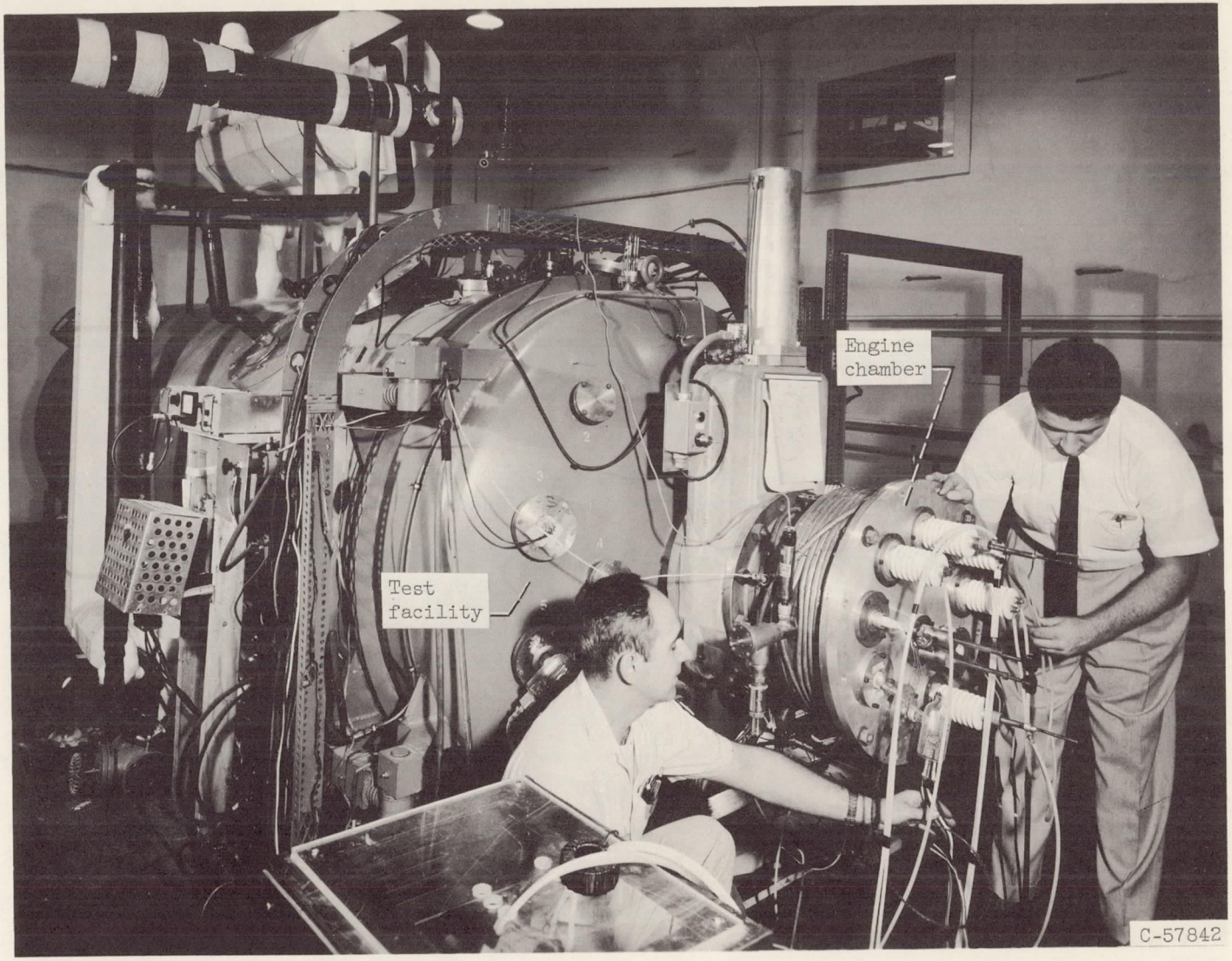

Figure 1. - Typical facility used for tests.

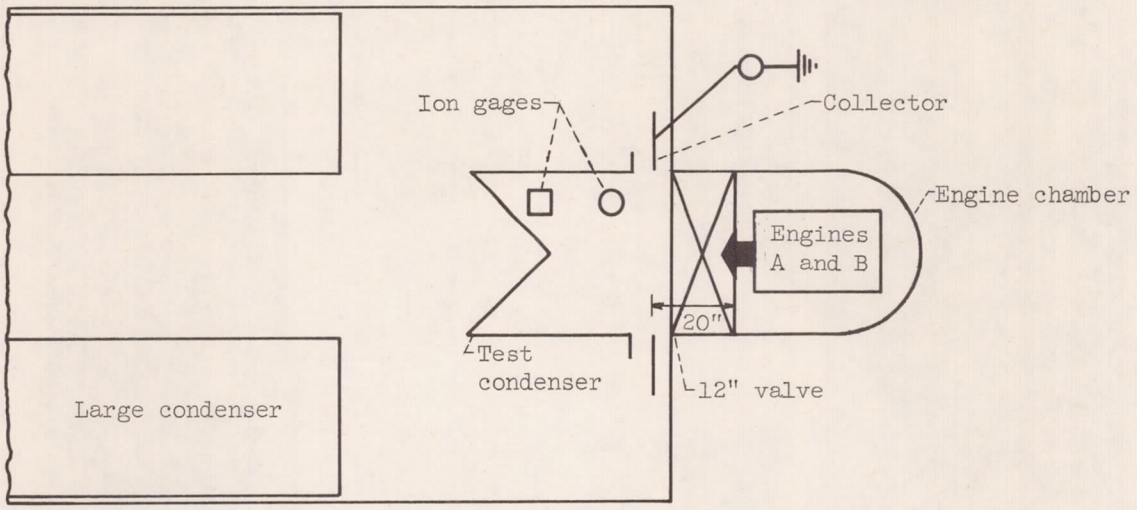

(a) Engines A and B.

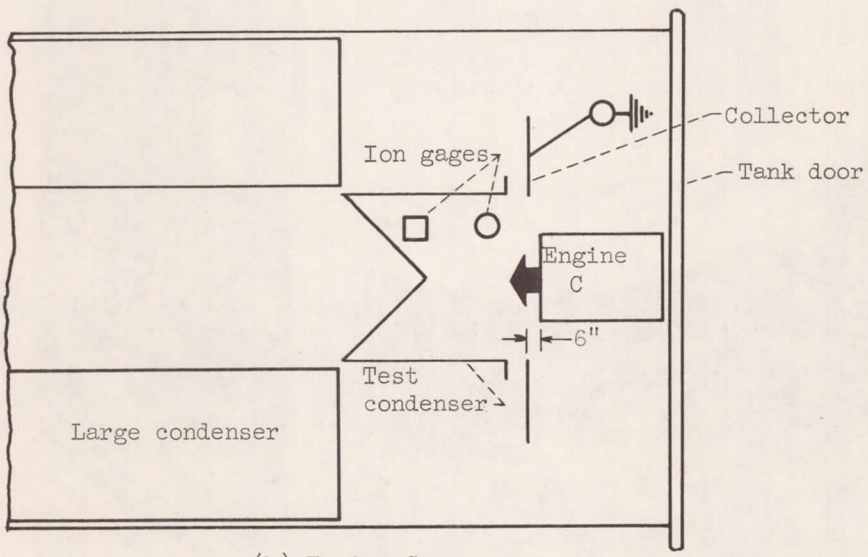

(b) Engine C.

Figure 2. - Engine test setup.

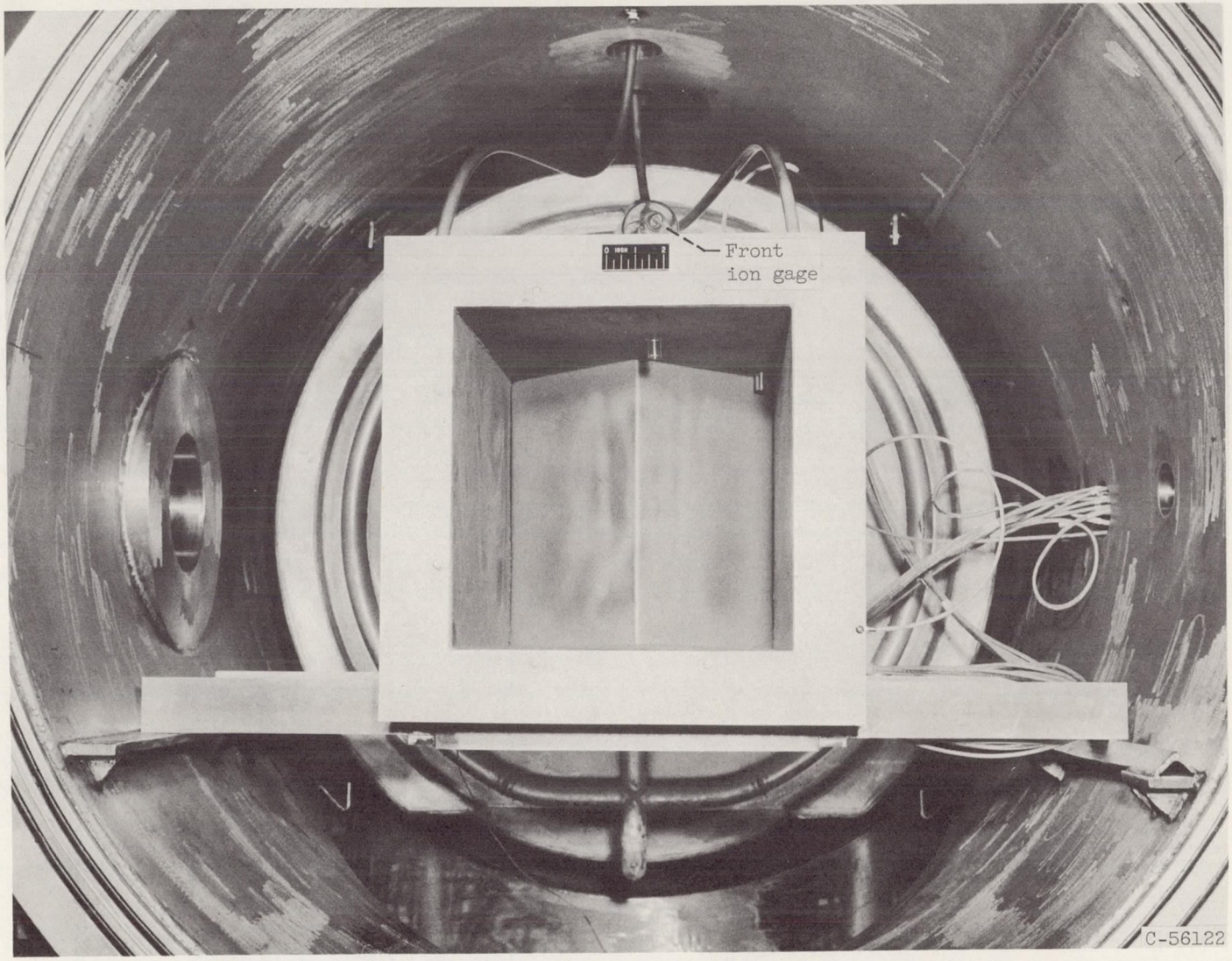

(a) Typical, plain-wall condenser. S_1, 0.64 square meters; S_5, 0.27 square meters.

Figure 3. - Condensers.

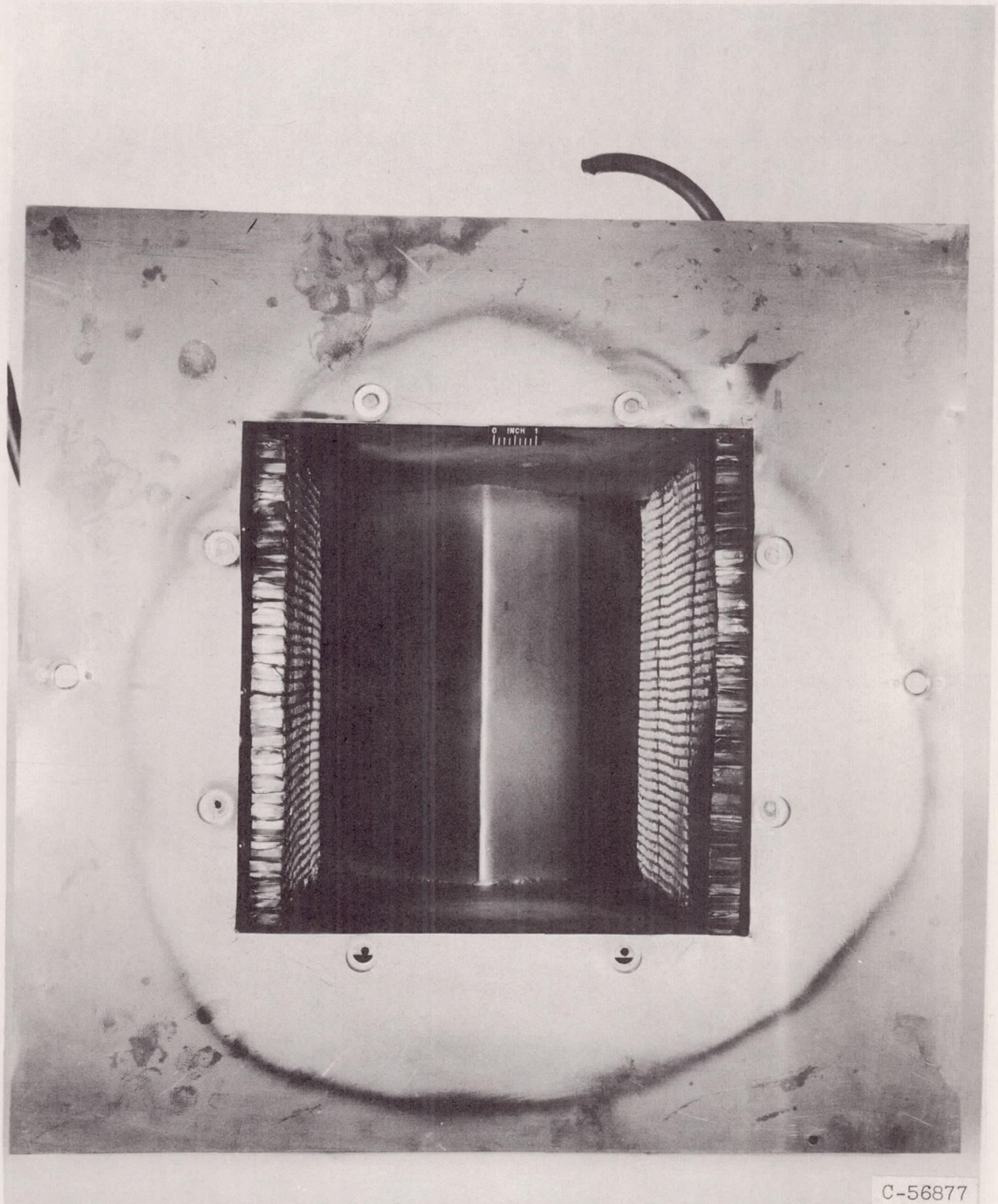

(b) Partial-honeycomb condenser. S_2, 2.86 square meters. Ion gages not shown.

Figure 3. - Continued. Condensers.

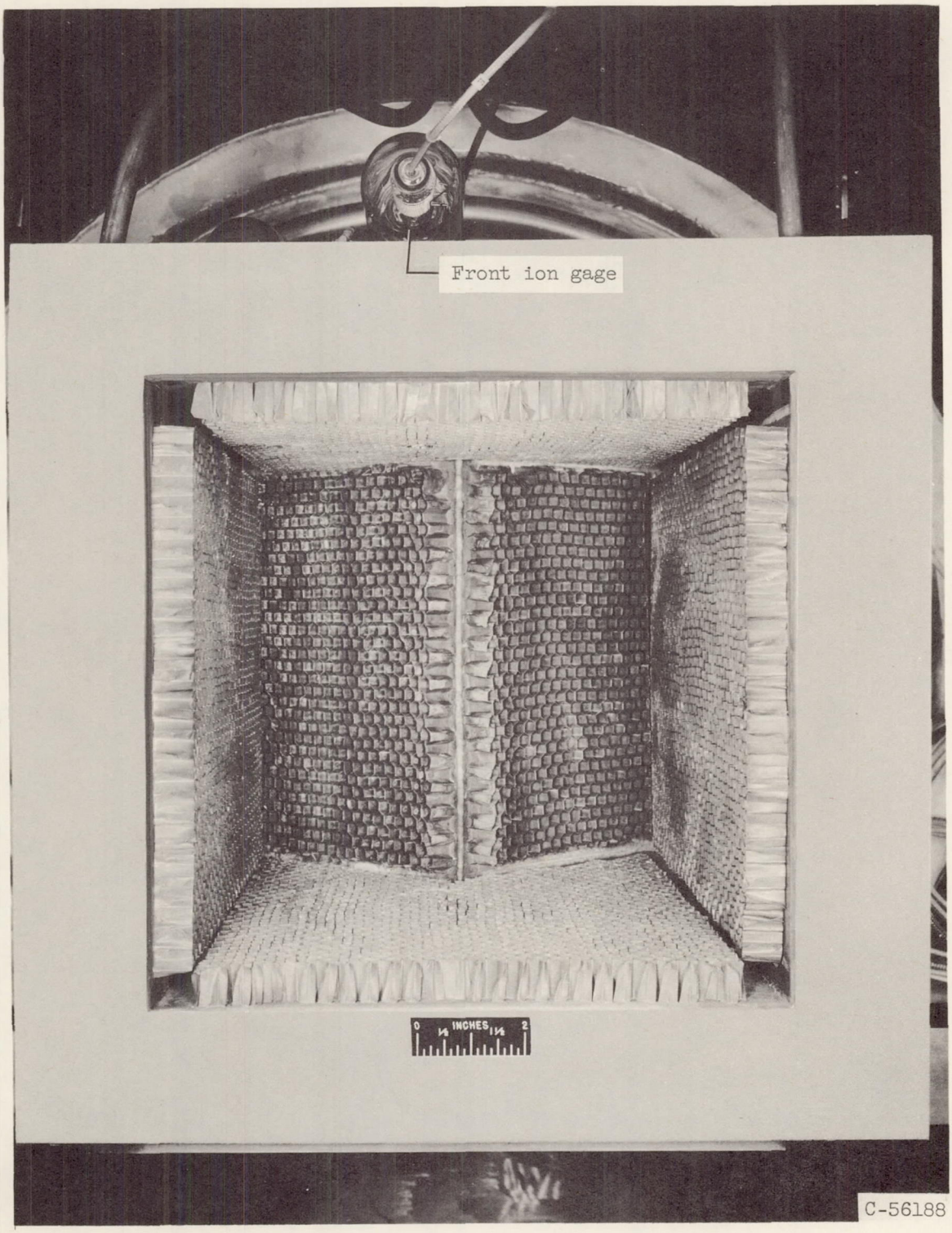

(c) Full-honeycomb condenser. S_3, 5.76 square meters.

Figure 3. - Continued. Condensers.

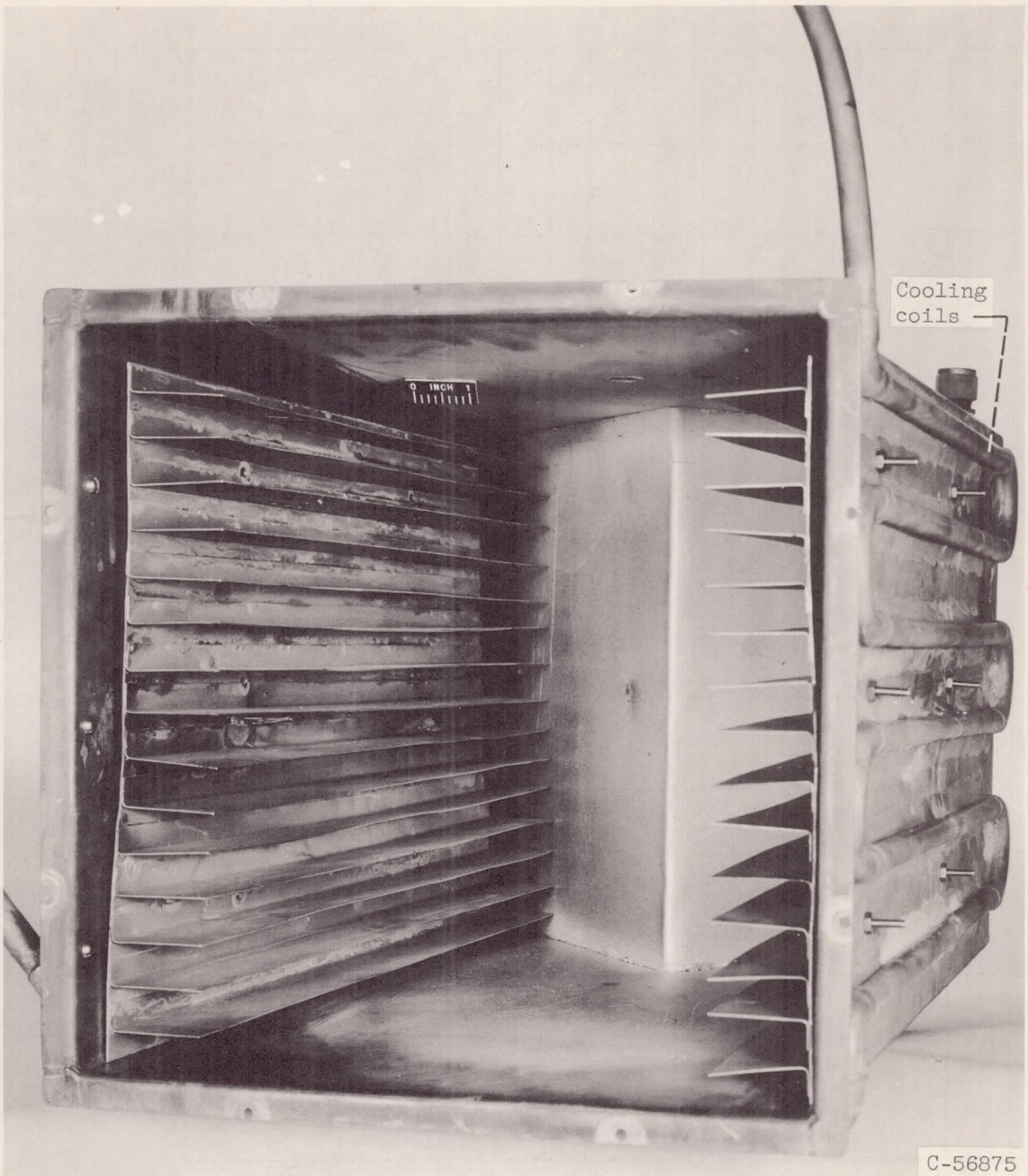

(d) Finned condenser. S_4, 1.57 square meters. Ion gages not shown.

Figure 3. - Concluded. Condensers.

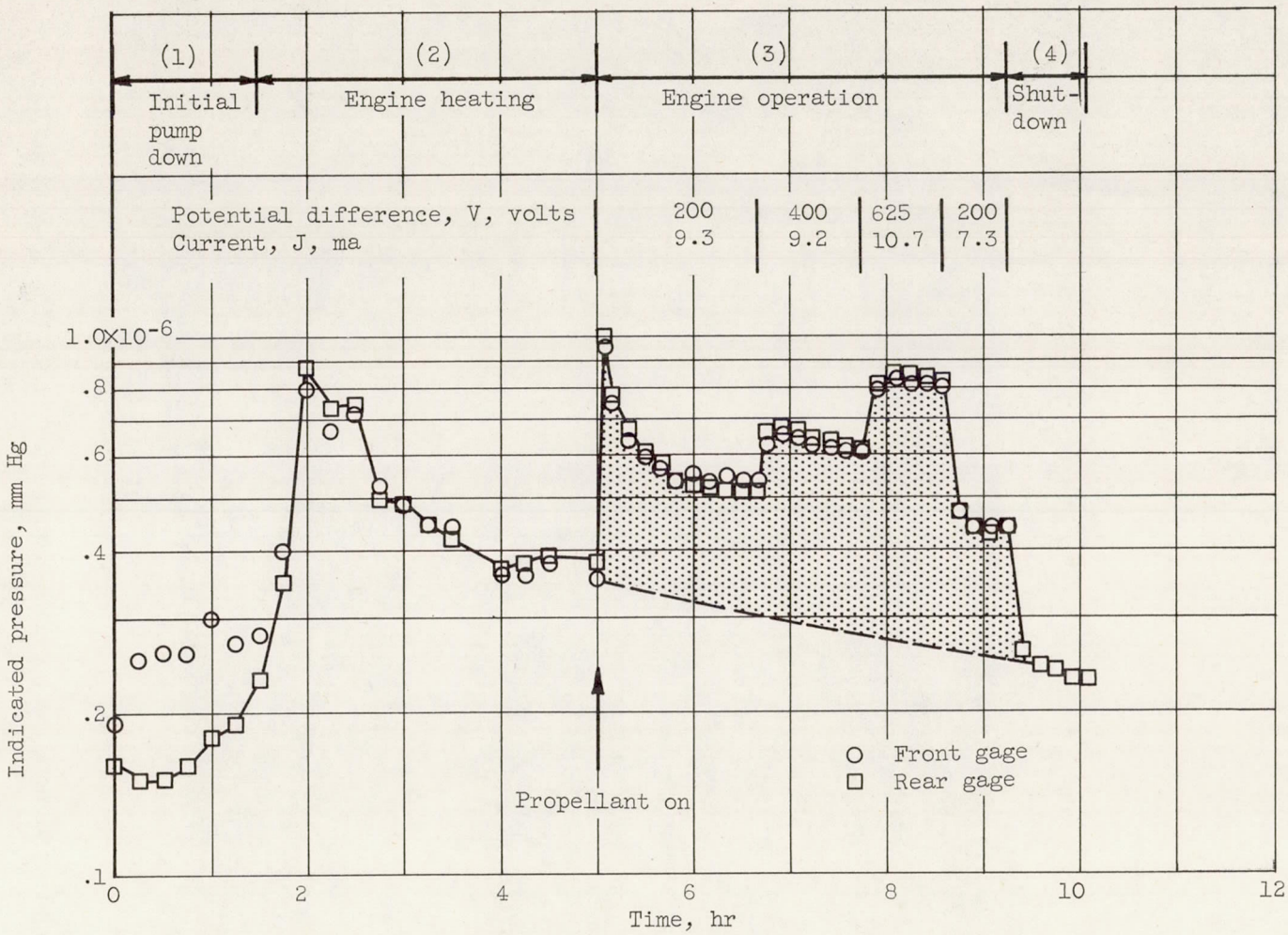

(a) Engine A.

Figure 4. - Typical variation of pressure with time for engines A and C with S_1 condenser.

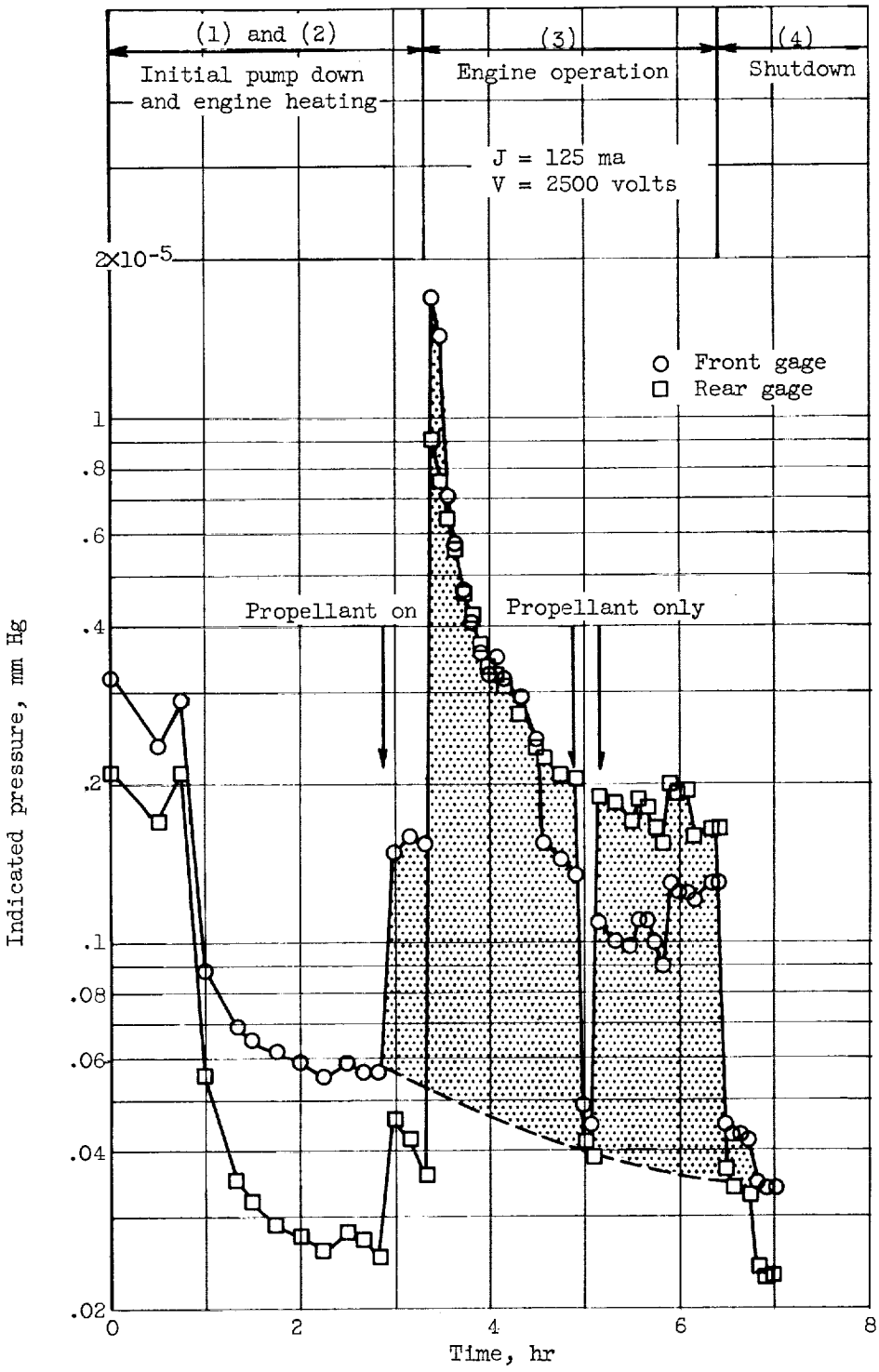

(b) Engine C.

Figure 4. - Concluded. Typical variation of pressure with time for engines A and C with S_1 condenser.

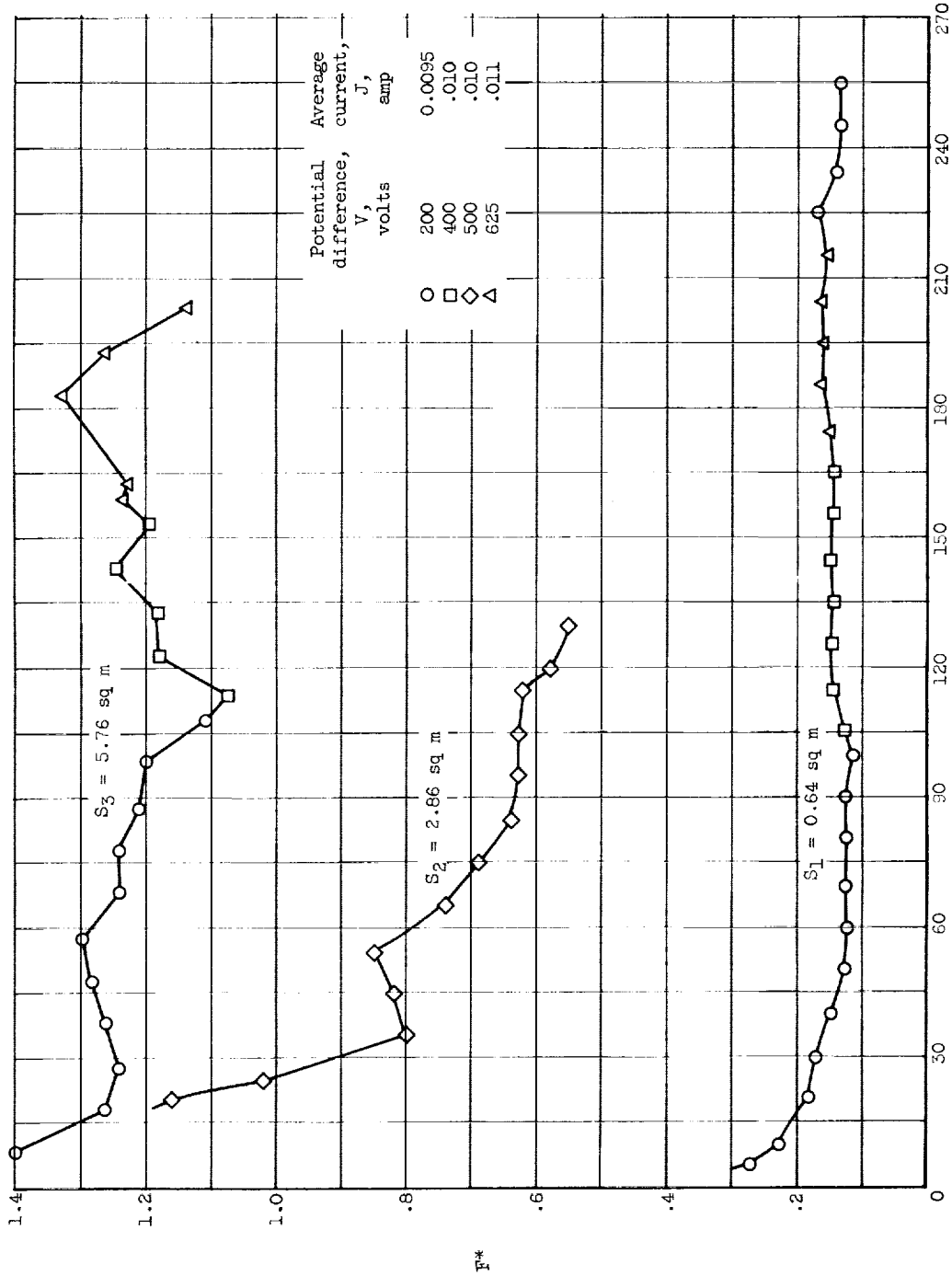

(a) Engine A tests. Current, 0.007 to 0.012 ampere.

Figure 5. - Variation of F* with time. Liquid-nitrogen cooling.

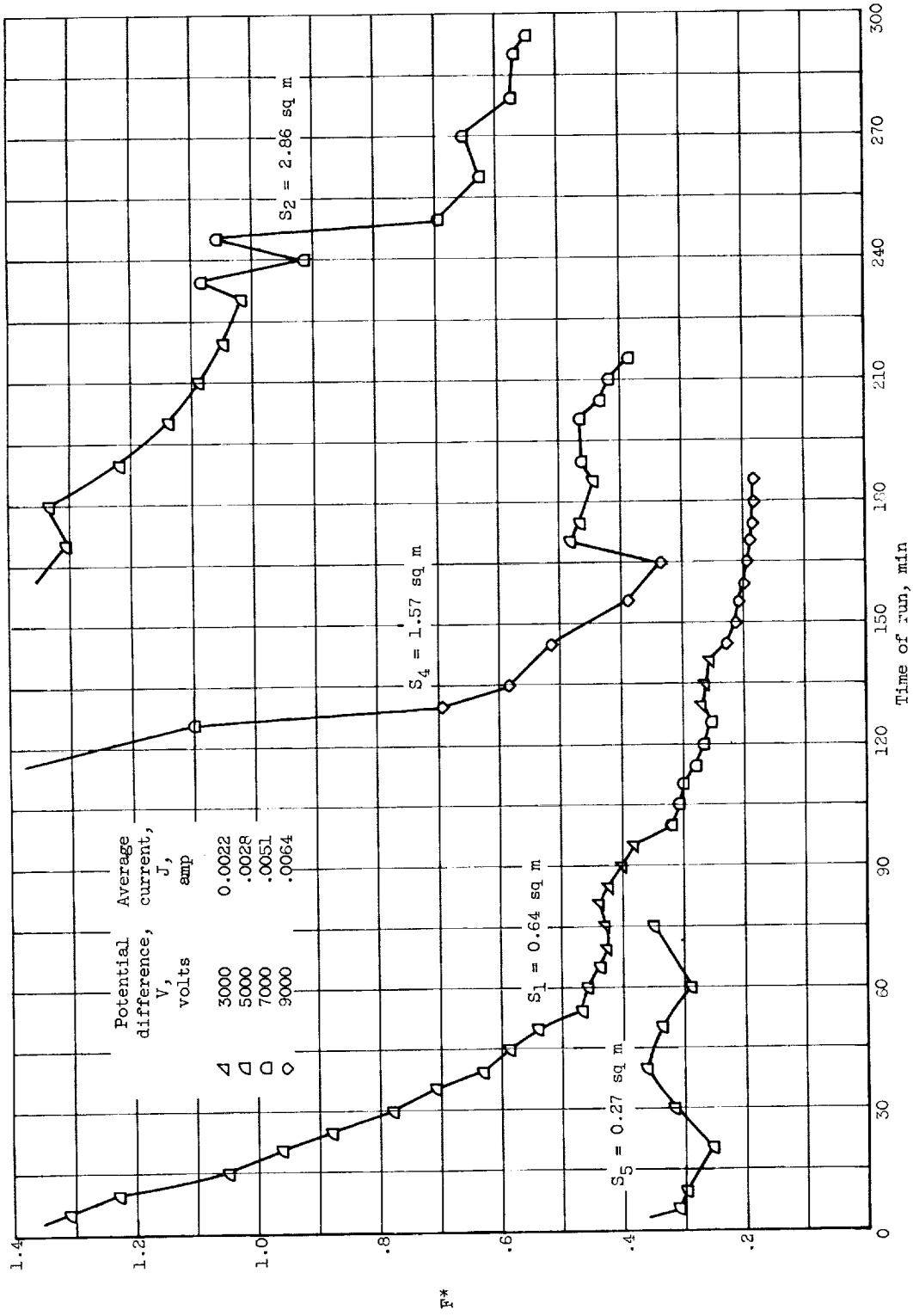

(b) Engine B tests. Current, 0.002 to 0.007 ampere.

Figure 5. - Continued. Variation of F* with time. Liquid-nitrogen cooling.

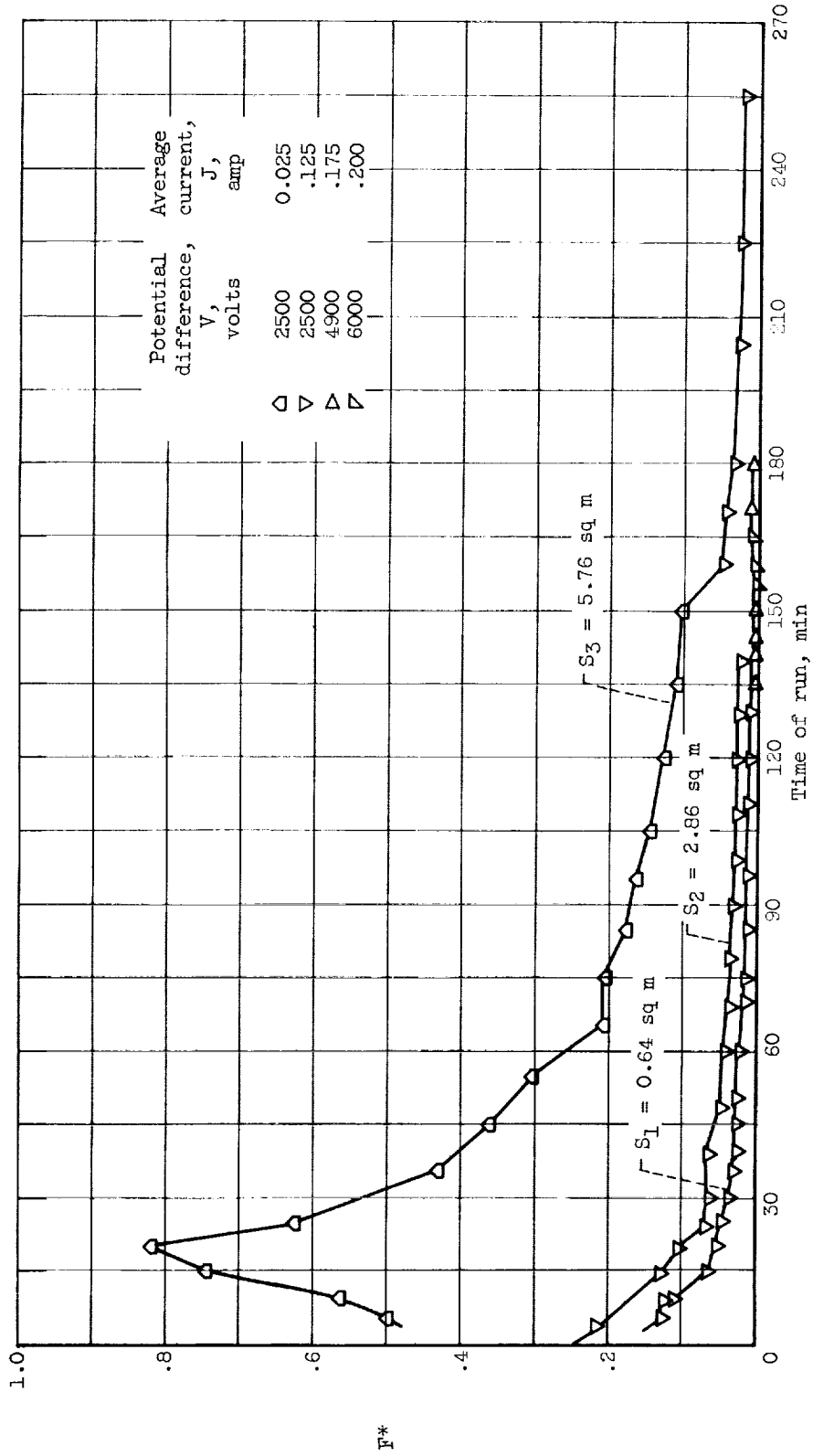

(c) Engine C tests. Current, 0.025 to 0.200 ampere.

Figure 5. - Concluded. Variation of F* with time. Liquid-nitrogen cooling.

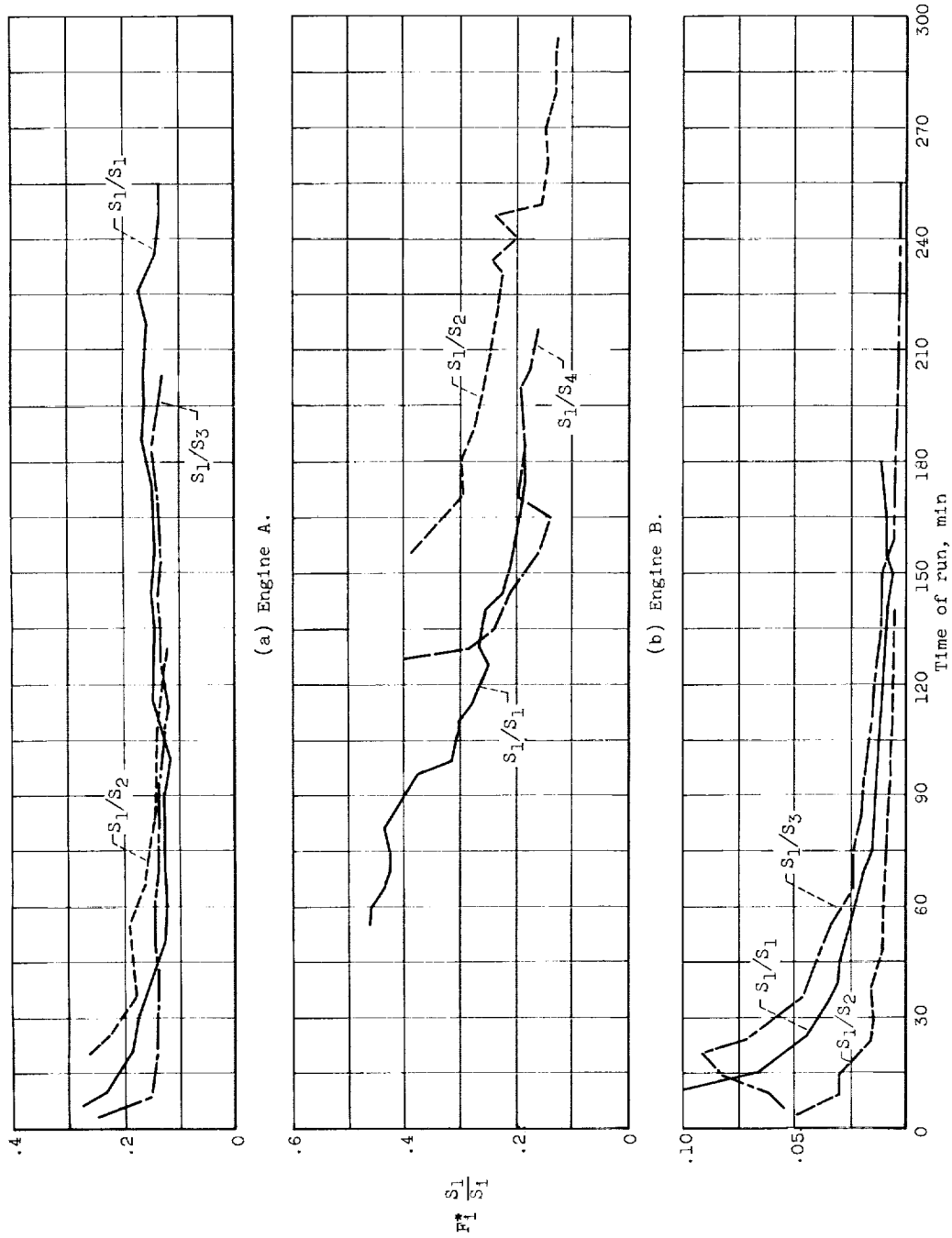

Figure 6. - Variation of $\left(F^* \frac{S_1}{S_1}\right)$ with time for engines A, B, and C.

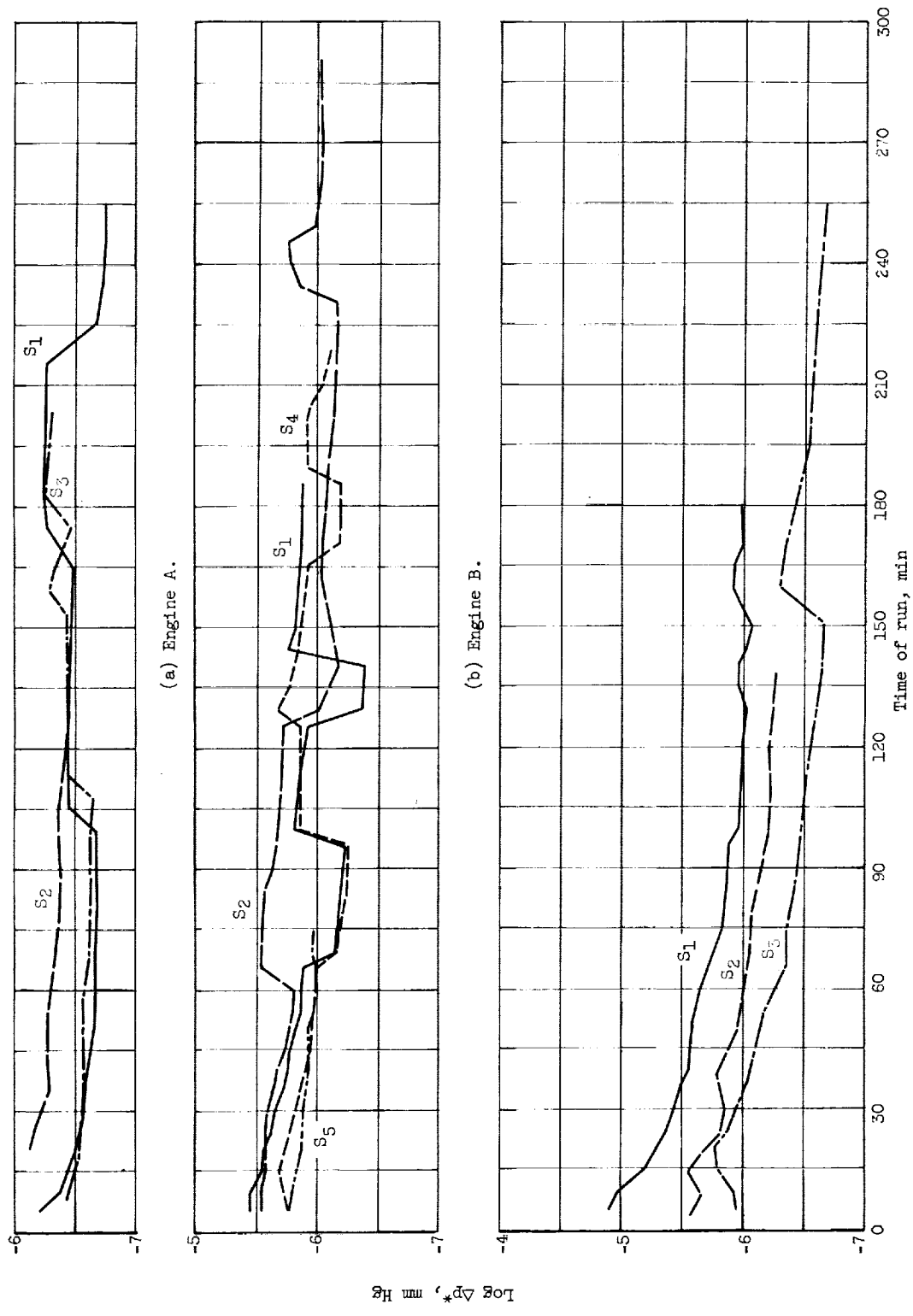

Figure 7. - Variation of indicated pressure differential with time for engines A, B, and C.

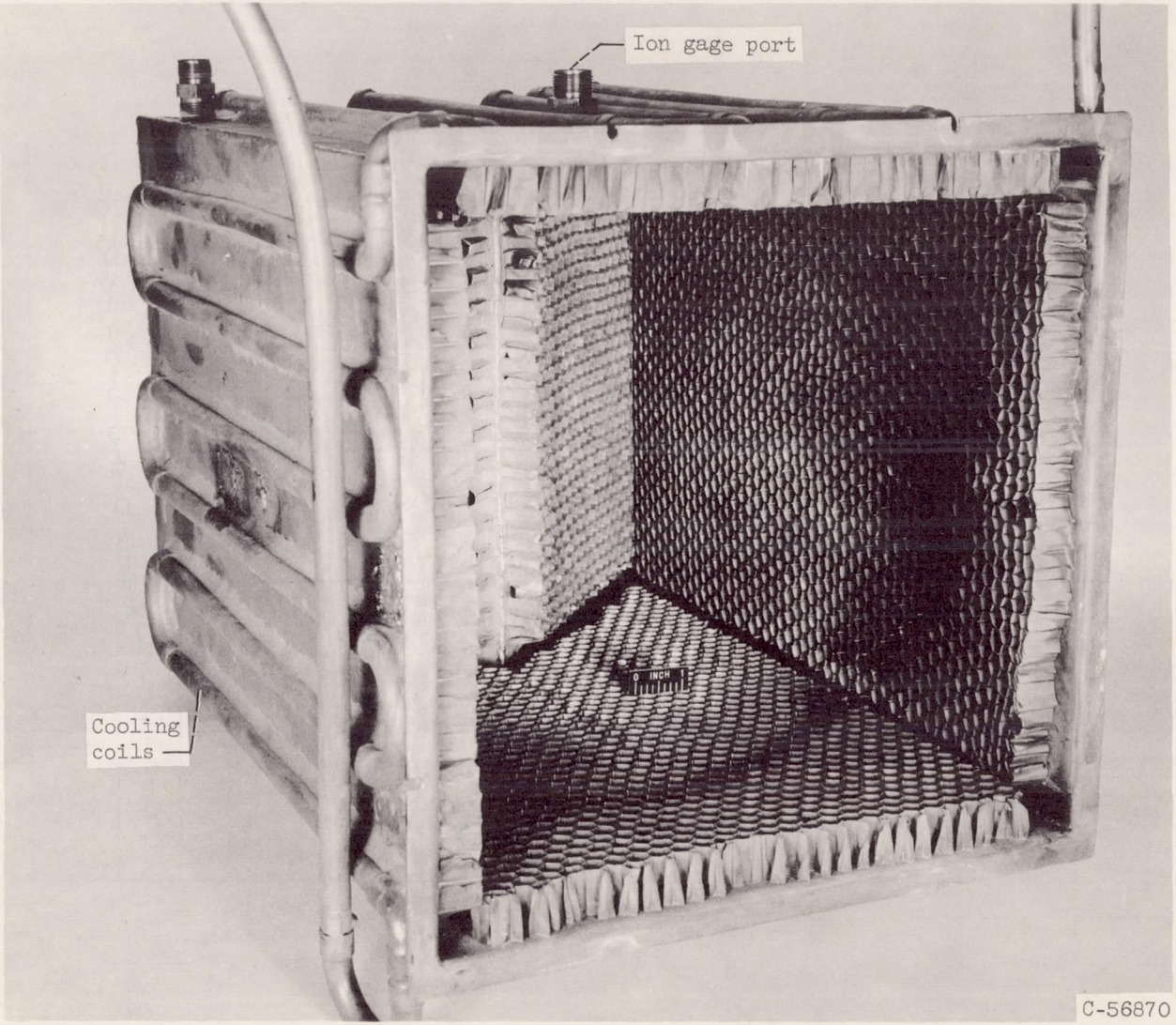

Figure 8. - Condenser S_3 after test with engine C.

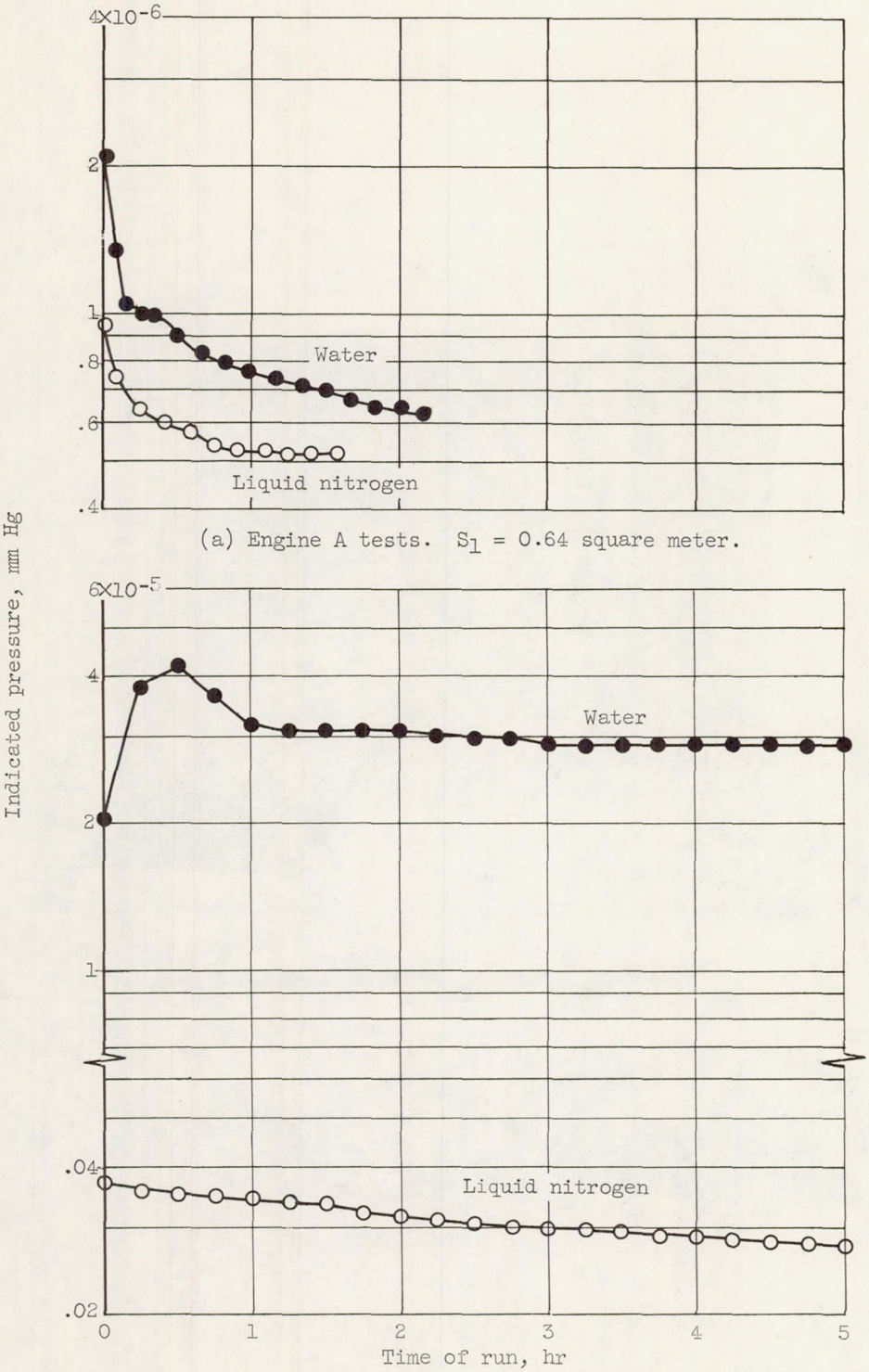

(a) Engine A tests. S_1 = 0.64 square meter.

(b) Engine C tests. S_2 = 2.86 square meters.

Figure 9. - Comparison of liquid nitrogen versus water as a coolant (step (3) only).

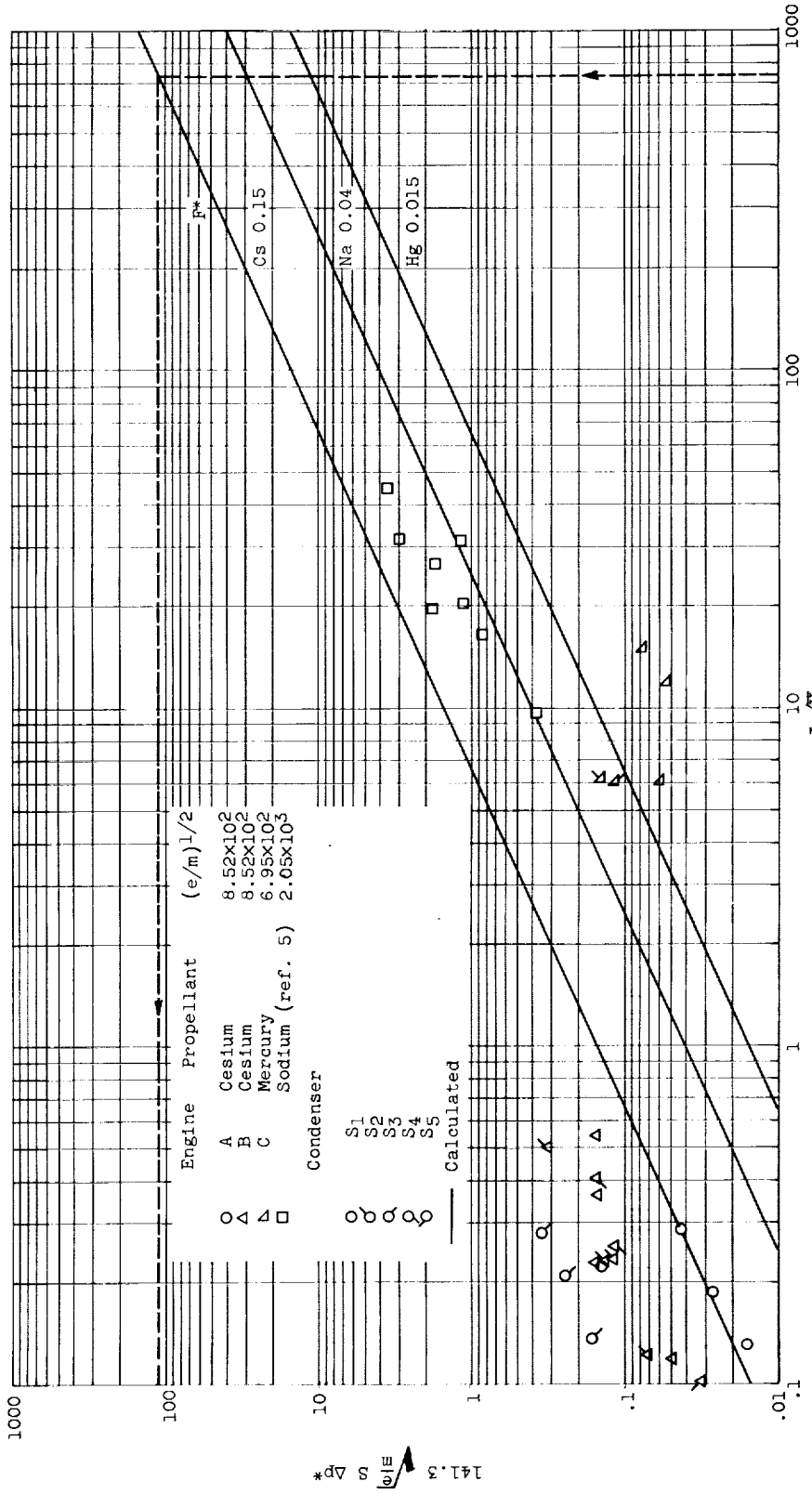

Figure 10. - Summary plot of data.